Research Article | Vol. 26, No. 23 | 12 Nov 2018 | OPTICS EXPRESS 30042
Optics EXPRESS

Photonic lantern broadband orbital angular momentum mode multiplexer

ZEINAB SANJABI EZNAVEH,[1,*] JUAN CARLOS ALVARADO ZACARIAS,[1] JOSE ENRIQUE ANTONIO LOPEZ,[1] KAI SHI,[2] GIOVANNI MILIONE,[3] YONGMIN JUNG,[4] BENN C. THOMSEN,[2] DAVID J. RICHARDSON,[4] NICOLAS FONTAINE,[5] SERGIO G. LEON-SAVAL,[6,7] AND RODRIGO AMEZCUA CORREA[1]

[1]*CREOL, the College of Optics and Photonics, University of Central Florida, Orlando, Florida 32816, USA*
[2]*Optical Networks Group, University College London, London WC1E 7JE, UK*
[3]*NEC Laboratories America, Inc. Princeton, NJ 08540, USA*
[4]*Optoelectronics Research Center, Southampton University SO17 1BJ, UK*
[5]*Nokia, Bell Labs, Holmdel, NJ 07733, USA*
[6]*Sydney Astrophotonic Instrumentation Laboratory, School of Physics, University of Sydney, NSW 2006, Australia*
[7]*Institute of Photonics and Optical Science, School of Physics, University of Sydney, NSW 2006, Australia*
**Zahoora@knights.ucf.edu*

Abstract: Optical vortex beams that carry orbital angular momentum (OAM), also known as OAM modes, have attracted considerable interest in recent years as they can comprise an additional degree of freedom for a variety of advanced classical and quantum optical applications. While canonical methods of OAM mode generation are effective, a method that can simultaneously generate and multiplex OAM modes with low loss and over broad spectral range is still in great demand. Here, via novel design of an optical fiber device referred to as a photonic lantern, where the radial mode index ("m") is neglected, for the first time we demonstrate the simultaneous generation and multiplexing of OAM modes with low loss and over the broadest spectral range to date (550 nm). We further confirm the potential of this approach to preserve the quality of studied OAM modes by fusion splicing the end-facet of the fabricated device to a delivery ring-core fiber (RCF).

1. Introduction

Light beams can have orbital angular momentum (OAM). In contrast to spin angular momentum, which is associated with the state of polarization, OAM is associated with the light beam's phase front. A light beam that has an azimuthally varying phase front given by $\exp(il\phi)$, is referred to as an optical vortex which has an OAM of $l\hbar$ per photon where, $l = 0, \pm1, \pm2, \ldots$ is the topological charge number, ϕ is the azimuthal angle, and $\hbar$ is the reduced Planck constant [1,2].

OAM modes comprise a high-dimensional and complete set of orthonormal solutions of the paraxial wave equation with which to represent the space degree of freedom of light. As such, there is interest in the use of OAM modes or a superposition thereof, for various applications in both classical and quantum physics studies. For example, it is possible to use OAM modes to increase the data speeds of free space and optical fiber communications via mode division multiplexing [3–6] and amplitude multiplexing [7] and enhance the security of quantum cryptography via high-dimensional quantum key distribution [8–10]. In addition, OAM modes or their superposition, provide a high-dimensional resource for fundamental tests of quantum mechanics such as quantum entanglement [11–14], and can be used for

#342351 https://doi.org/10.1364/OE.26.030042
Journal © 2018 Received 14 Aug 2018; revised 30 Sep 2018; accepted 16 Oct 2018; published 31 Oct 2018

Optics EXPRESS

novel methods of remote sensing [15], high-resolution imaging [16,17] and high-precision optical measurements [18,19].

Essential to the applications above is the ability to multiplex OAM modes, i.e., combining multiple OAM modes into a single light beam, with low loss and over a broad range of wavelengths. Multiplexing is possible by using canonical methods to generate OAM modes, such as liquid crystal based spatial light modulators and so-called q-plates [20–22], in concert with beam splitters. However, this unavoidably incurs a 1/N loss of power, where N is the number of OAM modes multiplexed. While more advanced methods to generate OAM modes were demonstrated, i.e., direct generation from laser cavities, and micron sized silicon based ring resonators [23–25], a major challenge is the ability to multiplex OAM modes with low loss. More recently, it was shown that OAM modes can be multiplexed using multi-plane light conversion and log to polar geometric transformation [26], however, operating over a limited range of wavelengths. Therefore, there is need of a broadband and low loss method to multiplex OAM modes.

In this work, we report on the first demonstration of an extremely broadband and low loss OAM mode multiplexer/de-multiplexer (MUX/DEMUX). The proposed OAM mode MUX is based on a modified optical device, referred to as a mode selective photonic lantern (MSPL) [27–35]. This new MSPL has an engineered ring-shape refractive index profile, designed to be compatible with well-stablished OAM delivery ring-core fibers (RCFs) [36–38]. This yields efficient mode coupling to RCFs and low insertion loss. Through simultaneous excitation of the pairs of degenerate LP modes of the MSPL, we can explicitly generate high quality OAM modes with topological charge numbers -up to the second order. Additionally, we demonstrate a proof-of-concept experiment that validates simultaneous multiplexing of multiple orthogonal OAM modes in a single fiber device. This innovative all-fiber device potentially shows low loss with low design complexity; therefore, it is of grand utility in variety of applications in classical, quantum and modern optical studies.

2. Method

2.1 Experimental realization

We exploit the mode-selective behavior of a specialty annular-index MSPL to achieve an all-fiber connectorized OAM mode MUX/DEMUX. A detailed fabrication process of a standard MSPL mode MUX/DEMUX has been described elsewhere [27,39,40]. Here, we briefly review the main fabrication procedure. A standard MSPL consists of an array of isolated dissimilar few-mode fibers (FMFs) inserted inside a low refractive index capillary. The whole structure is then adiabatically tapered such that the FMF cores reduce in size and nearly disappear. As a result, the FMF cladding becomes the new multimode fiber (MMF) core with the low-index capillary behaving as its cladding. Since the propagation constants of each input FMF are distinct, different modal evolution along the tapered transition is achieved. Hence, the fundamental mode of each input fiber can evolve into one specific mode or mode group combination of the output MMF. If the transition is adiabatic, the modes of the MMF core evolve into the modes of the FMF array, and vice versa.

The scalar modes of a MSPL mode MUX/DEMUX are composed of two vector eigenmodes with different propagation constants [41], i.e., $LP_{lm} = HE_{(l+1)m} + EH_{(l-1)m}$. Here, l refers to the mode order in azimuthal direction and $m(>=1)$ refers to the mode order in radial direction. Regardless of the polarization term, for $l(>=1)$, all LP_{lm} modes are two-fold degenerate as odd and even configurations. By combining a pair of degenerate LP_{lm} modes with a phase difference of $\pm\pi/2$, one can obtain two degenerate $OAM_{\pm l}$ modes with opposite sign of topological charge numbers. Figure 1 illustrates the intensity and phase profiles of the $OAM_{\pm l}$ modes ($l = 0, 1, 2$) achieved from the superposition of the pairs of degenerate LP modes of a 5-mode MSPL.

Optics EXPRESS

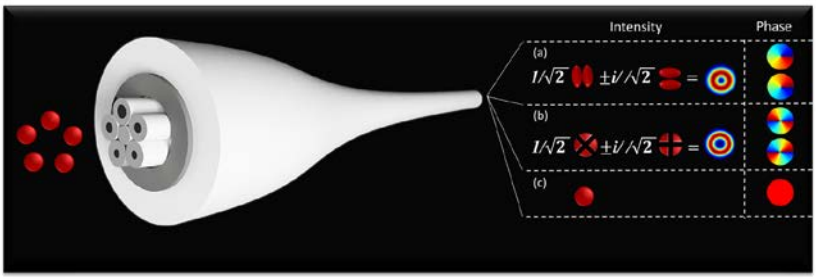

Fig. 1. Superposition of degenerate LP_{l1} modes of a 5-mode MSPL to generates OAM modes and their corresponding +/– helical phase patterns with (a) l = 1, (b) l = 2 and (c) l = 0 corresponding to LP_{01} mode.

2.2 Design and fabrication of the delivery RCF

The primary aim of using a RCF is to remove the near-degeneracy of the *HE* and *EH* vector modes, hence, to suppress inter-mode cross talk and preserve OAM modes along propagation [5,38]. OAM modes in such fibers are composed of fiber eigenmodes with equal propagation constants $(OAM_{\pm l} = HE^{even}_{(l+1)m} \pm i \times HE^{odd}_{(l+1)m})$. Figs. 2(a) and 2(b) show a microscope image of the cross section of the fabricated RCF which can support OAM modes of the first and second kinds, and its measured refractive index profile, respectively. The inner and outer diameters of the RCF are 7 μm and 18 μm, respectively. The cladding diameter is 123 μm, while the maximum core-clad refractive index contrast is 0.016. Numerically calculated effective index differences (Δn_{eff}) of all supported vector modes with respect to the LP_{01} mode at spectral range of 980 nm-1015 nm and over the full C-band (1530 nm-1565 nm) are represented in Fig. 2(c) and 2(d), respectively.

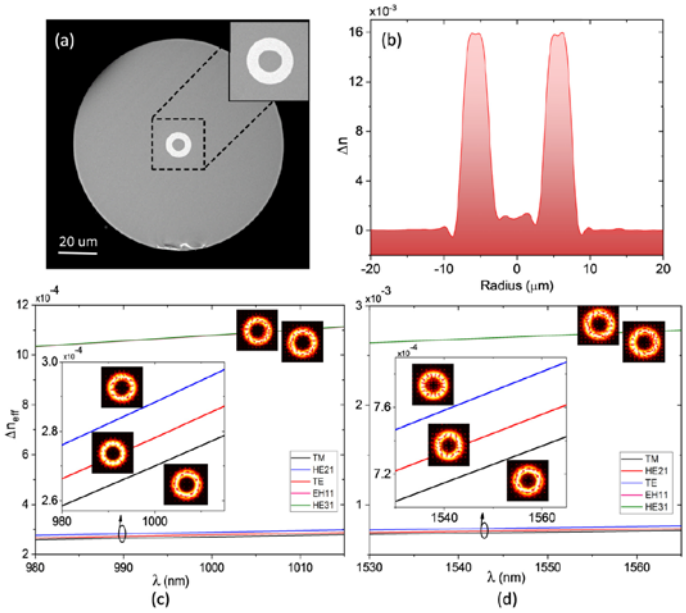

Fig. 2. (a) Microscope image of the cross section of the fabricated RCF with ring inner/outer diameter of 7 μm / 18 μm and fiber outer diameter of 123 μm. (b) Measured refractive index profile of the RCF at 660 nm. (c) Calculated effective index differences of the supported vector modes with respect to the LP_{01} mode at 980 nm-1015 nm and (d) across the C-band (1530 nm-1565 nm).

Optics EXPRESS

According to our simulations using a finite-element mode solver (COMSOL), a maximum separation of the order of 10^{-5} between the effective indices of TM_{01} mode and HE_{21} mode and a value of 10^{-4} between the effective indices of the HE_{31} mode and EH_{11} are obtained.

3. Results

3.1 Demonstration of an annular OAM mode MUX

To efficiently transmitting the OAM modes of the mode generator into a delivery RCF, one should assure high coupling efficiency between the two fiber components. In practice, this can be achieved by appropriately designing the OAM mode MUX to perfectly mode match the delivery RCF, i.e. a ring-core mode MUX. This unique engineered design preserves OAM mode quality while performing fusion splicing between two fiber devices. Besides, it reduces modal dependent loss and device complexity whilst enhancing operational stability and device flexibility.

To fabricate a ring-core OAM mode MUX, we follow the same procedure as for the aforementioned standard MSPL except for replacing the central core by a core-less fluorine-doped fiber. This fiber has a core diameter of 86 μm and a refractive index contrast of -9×10^{-3} with respect to the background glass in order to form a null intensity profile in the center. This is the key feature of our ring-shaped OAM mode MUX, which leads to exceptionally reliable mode-match, hence, providing low-loss and stable transformation of the OAM modes into the delivery RCF. Figure 3(a) shows the microscope image of the end facet of the fabricated device, while the inset shows its schematic representation. The ring inner diameter *a*, ring outer diameter *R* and clad inner/outer diameters ID/OD are 6 μm, 28 μm and 90 μm/125 μm, respectively. In addition, Figs. 3(b)-3(d) display the experimentally obtained near field intensity profiles of the excited modes at the output of the OAM mode MUX at 1000 nm and 1550 nm, respectively. The obtained high quality *LP* modes at broad spectral range of at least 550 nm (limited to the range of the available laser diodes) are indication of the effective design and fabrication precision of these device.

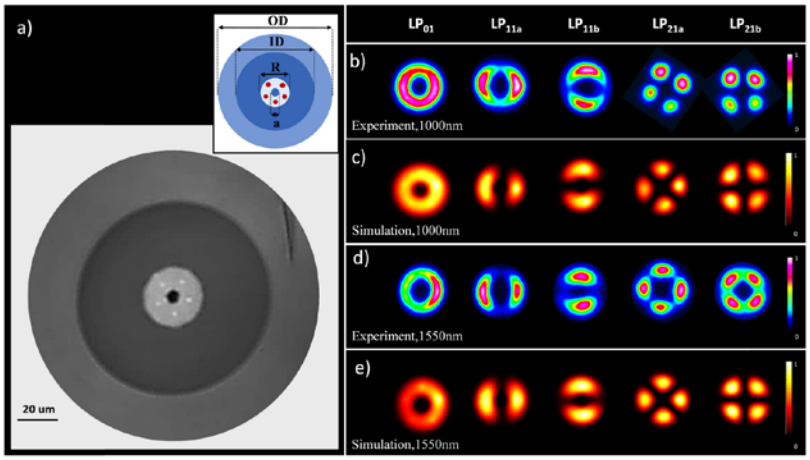

Fig. 3. (a) Microscope image of the cross section of the OAM mode MUX. (Inset) Schematic cross section of the fabricated device, a = 6 μm, R = 28 μm, ID = 90 μm and OD = 125 μm. (b) Measured, and (c) simulated near field mode profiles of the OAM mode MUX at 1000 nm. (d) Measured, and (e) simulated near field mode profiles of the OAM mode MUX at 1550 nm.

In order to further corroborating the performance of the fabricated OAM mode MUX, the output mode profiles were calculated using COMSOL. As it is clear from Figs. 3(c)-3(e), there is an excellent agreement between the experimental results and numerical simulations. The slight variations between the calculated and measured modes are a product of the small

Optics EXPRESS

geometry deformation of the final fabricated core at the multimode end of the OAM photonic lantern.

3.2 Generation and detection of the OAM beams

The schematic representation of the experimental setup used for generation and detection of the OAM modes based on the proposed all-fiber OAM mode MUX is shown in Fig. 4. A standard single mode fiber at the output of a 1550 nm (or 1000 nm) laser diode is directly spliced onto a 50:50 optical coupler. One port of the 50:50 coupler is used to deliver a reference Gaussian beam to the interferometer to later verify the generation of the OAM beams. The other port of the coupler is spliced to a second 50:50 coupler whose output ports are then spliced to the $LP_{11\,a,b}$ (or $LP_{21\,a,b}$) ports of the OAM mode MUX. A 20x microscope objective and a CCD camera are used to capture the output beam. By simultaneously exciting the two ports of the degenerate $LP_{11\,a,b}$ (or $LP_{21\,a,b}$) modes, we obtain a ring-shaped mode profile at the output facet of the OAM mode MUX. It should be clearly emphasized that the required phase difference of $\pm\pi/2$ to generate OAM beams was feasibly and easily provided by using a polarization controller in one arm of the degenerate *LP* modes, as shown in Fig. 4.

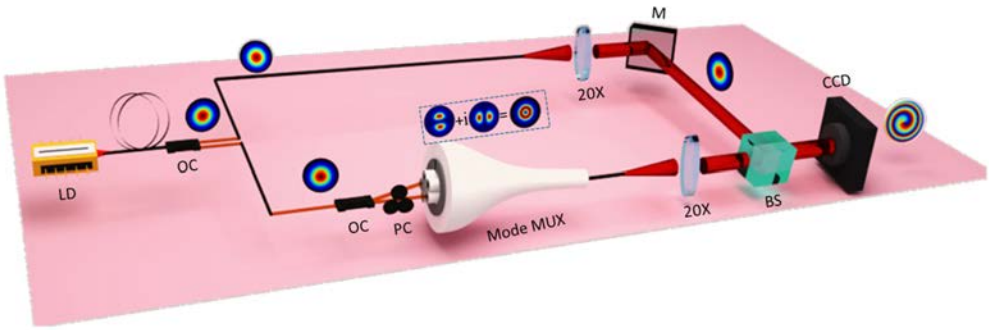

Fig. 4. Schematic of the experimental setup for generation and detection of OAM modes. LD, laser diode; SMF, single-mode fiber; OC, 3-dB optical coupler; PC, polarization controller; Mode-Mux, OAM mode multiplexer; M, mirror; BS, beam splitter.

Figure 5 illustrates the near field intensity profiles of the generated OAM_l modes (with $l = \pm 1, \pm 2$) at the output of the fabricated device at 1000 nm [Figs. 5(a) and 5(b)] and 1550 nm [Figs. 5(c) and 5(d)], respectively. In order to reveal and further prove the phase singularity of the OAM modes and identify the mode orders, we recorded the interference pattern of the output beam of the OAM mode MUX with a reference uniformly polarized Gaussian beam. High-quality ring-shape intensity profiles and clean spiral interferograms displayed in Fig. 5 indicate effective conversion of the *LP* modes to high purity OAM states.

To verify the low loss and stable transmission of the generated OAM modes, we spliced the end facet of the OAM mode MUX into a 1 m long RCF represented in Fig. 2(b). As mentioned earlier, the core diameter and the ring thickness of the RCF were designed to mode-match the final core size of the OAM mode MUX. The insertion loss of the fabricated mode MUX/DEMUX is found to be less than 3 dB.

Figure 5 depicts the near field intensity distribution of the OAM modes at the output of 1 m long RCF and their interference patterns with the reference Gaussian beam at 1000 nm [Figs. 5(e) and 5(f)] and 1550 nm [Figs. 5(g) and 5(h)], respectively.

Optics EXPRESS

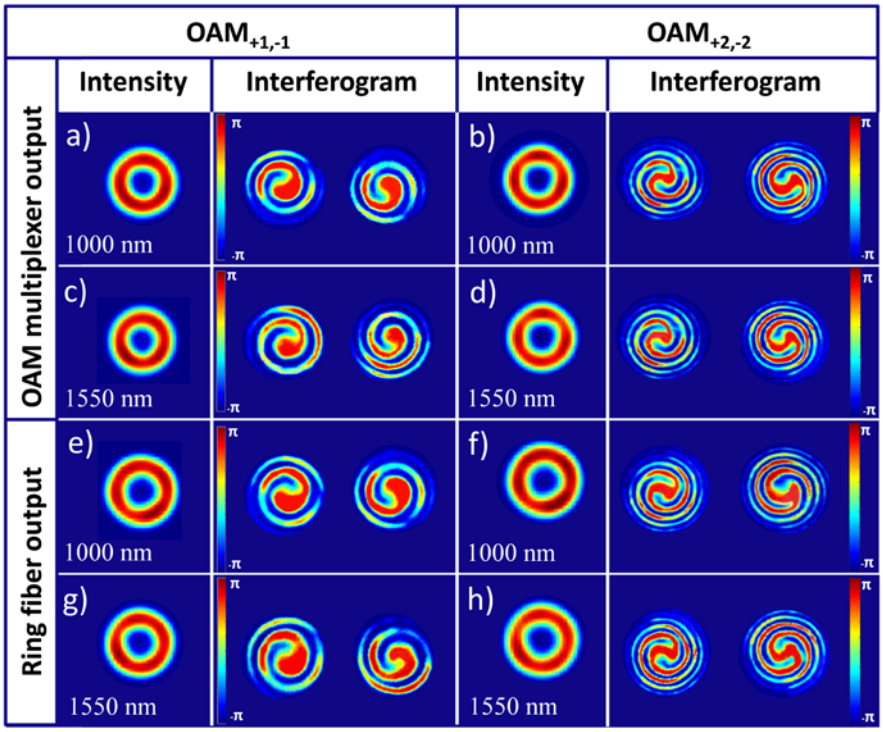

Fig. 5. Near field Intensity profiles and phase patterns of the generated OAM modes at the output of the fabricated OAM mode MUX at (a, b) 1000 nm and (c, d) 1550 nm. Intensity profiles and phase patterns of the generated OAM beams after 1 m propagation in a RCF at (e, f) 1000 nm and (g, h) 1550 nm.

The high quality OAM modes achieved at the output of the RCF accompanied by high purity spiral phase patterns, prominently indicate the effective generation and stable transmission of the OAM modes into the delivery fiber. Consequently, Fig. 5 confirms the broadband operational range of the fabricated device along at least 550 nm spectral bandwidth (1000 nm-1550 nm). To the best of our knowledge, this is the broadest range of operation of any OAM mode MUX reported so far.

3.3 Modal purity measurement

In order to estimate the mode selectivity of the fabricated device, a transmission system is set up, which uses two OAM photonic lanterns as the mode MUX/DEMUX (see Fig. 6). A 28 Gbaud dual-polarization, 16-ary quadrature amplitude modulated (16-QAM) signal with 2^{17} symbols is generated by using an IQ (in-phase and quadrature) modulator and a polarization MUX. This training signal is split and decorrelated by certain fiber delays to construct five decorrelated training sequences, each of which is then modulated and launched into the RCF. Both 1 km and 1 m (back-to-back) of the RCF are spliced between the two mode MUX/DEMUX for channel estimations individually. As the three mode groups (LP_{01}, $LP_{11a,b}$ and $LP_{21a,b}$) propagate along 1 km RCF at different speed, the crosstalk at the mode MUX/DEMUX can be investigated separately [42]. Whereas, the aggregate mode dependent loss (MDL) of the MUX/DEMUX can be obtained from the back-to-back (1 m) configuration without considering the MDL of the RCF.

Optics EXPRESS

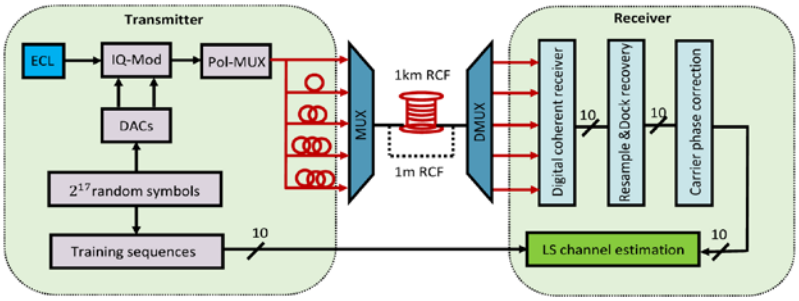

Fig. 6. Experimental setup and DSP algorithms for channel estimation. ECL: external cavity laser, IQ-Mod: in-phase and quadrature modulator, Pol-MUX: polarization multiplexer, DAC: digital-to-analogue converter, LS: least square

The least square algorithm is applied for the channel estimation [43]. The training sequences are first constructed digitally according to the decorrelation delays. A multi-channel digital coherent receiver captures the received waveforms with the information of the crosstalk arising from the mode MUX/DEMUX and distributed mode coupling along the fiber. The captured waveforms are then resampled to one sample per symbol with the sampling phase and laser phase noise correction. The amplitude of the estimated channel matrix of the transmission system over 1 km RCF is plotted in Fig. 7(a), where the values between the two polarizations are averaged. The discrete impulses represent the crosstalk either at the mode MUX or DEMUX. As we can see in the element h_{35} of the channel matrix, the impulse on the left hand side is arriving at the same time as launching LP_{11} modes (see the main impulse in h_{22}, h_{23}, h_{32}, h_{33}), which indicates that this impulse corresponds to the crosstalk from LP_{21b} mode to LP_{11b} mode at the mode MUX.

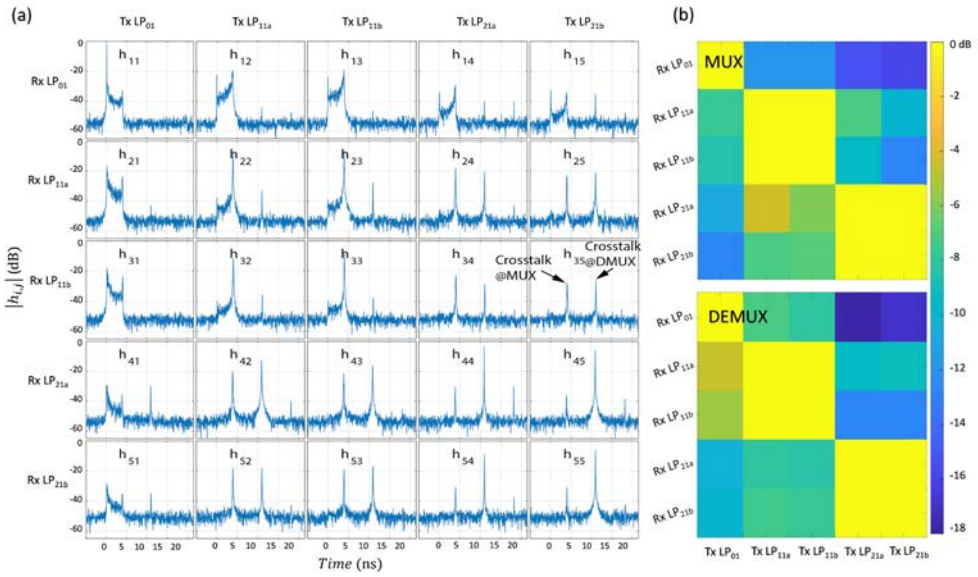

Fig. 7. (a) Channel impulse response of the transmission system over 1 km RCF using the photonic lanterns as the mode MUX and DEMUX. (b) Coupling matrices of the mode MUX and DEMUX.

On the other hand, for the impulse on the right hand side in element h_{35}, as it arrives at the same time as the LP_{21} modes (see the main impulse in h_{44}, h_{45}, h_{54}, h_{55}), it indicates that this impulse corresponds to the crosstalk from LP_{21b} modes to LP_{11b} mode at the mode DEMUX. By applying this analysis across the whole channel matrix and calculating the energy in these

Optics EXPRESS

discrete impulses, the coupling matrix of both mode MUX and DEMUX can be estimated separately. The results are shown in Fig. 7(b), demonstrating an average modal purity of >10 dB for all the modes.

Using the same technique, the channel matrix of the back-to-back configuration can also be obtained. Since the MDL between the modes in 1 m of the RCF is very small and can be neglected, by analyzing the eigenvalues of the back-to-back channel matrix, the MDL of the mode MUX/DEMUX is found to be 1.52 dB.

3.4 Simultaneous multiplexing of multiple OAM modes

Here, we perform a proof of-concept experiment that validates the idea of multiplexing of two OAM beams (OAM_{+1} + OAM_{-2}). To accomplish this, we split the input laser beam into 4 output divisions to simultaneously excite $LP_{11a,b}$ (to generate OAM_{+1}) and $LP_{21a,b}$ (to generate OAM_{-2}), with the same power ratio. Figures 8(a)-8(d) show the experimental and simulation results achieved by superposition of the two OAM beams, at 1000 nm and 1550 nm, respectively. To verify the charge of the generated OAM beams, interference between the output beam and a reference Gaussian beam is recorded, resulting in the interferograms indicated in Figs. 8(a)-8(c). Simulation results depicted in Figs. 8(b)-8(d) are in perfect agreement with the corresponding experimental observations. Owing to their inherent orthogonality, OAM beams provide an enhancement in capacity and spectral efficiency of optical communication networks.

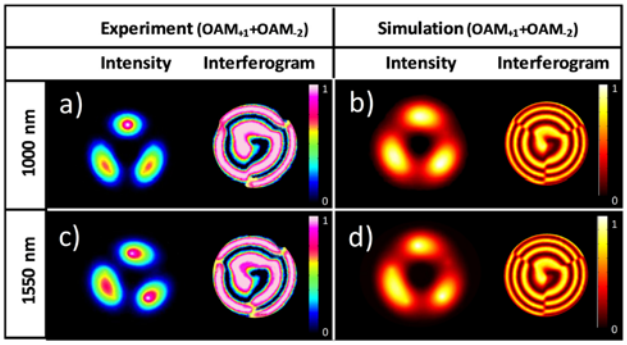

Fig. 8. (a, c) Measured, and (b, d) simulated near field mode profiles and interferograms of the generated OAM modes after multiplexing OAM_{+1} and OAM_{-2}, at 1000 nm and 1550 nm, respectively.

4. Summary

To develop a robust, reliable and passive approach to generate and preserve OAM modes, a new class of all fiber OAM mode MUX/DEMUX was presented and experimentally evaluated. The proposed device is a modified 5-mode MSPL with an annular refractive index profile. This engineered photonic lantern breaks the degeneracy of spatial modes in an optical fiber that is associated with “m,” i.e., the radial mode number therefore, enables OAM mode generation.

By simultaneously exciting the pairs of degenerate *LP* modes of the MSPL, we generated OAM modes up to the second order, with different topological charge numbers. The resulting high quality spiral phase patterns achieved from interference of the OAM beams with a reference Gaussian beam, verified generation of high purity OAM modes. Moreover, to indicate the stable and low-loss transmission of the generated OAM modes to a delivery fiber, we fusion spliced the end facet of the OAM mode MUX/DEMUX into a 1 m long RCF with equal structural parameters, and imaged the acquired interference pattern using a CCD camera. Achieving high quality OAM modes at the output of the RCF was successful due to the engineered design of the OAM mode MUX/DEMUX which efficiently mimics the field

Optics EXPRESS

structure of the OAM modes. The proposed all-fiber OAM mode MUX/DEMUX facilitates generation, multiplexing and transmission of OAM modes in a broad spectral range of at least 550 nm, which can be potentially used in widespread applications from classical optics to quantum physics studies.

Funding

National Science Foundation (NSF) (ECCS-1711230); Army Research Office (ARO) (W911NF-12-1-0450 and W911NF-17-1-0481); HEL-JTO (W911NF-12-1-0450); Air Force Office of Scientific Research (AFOSR) (FA955015-10041); U.K. Engineering and Physical Sciences Research Council (EP/J008842/1).

References

1. L. Allen, M. W. Beijersbergen, R. J. C. Spreeuw, and J. P. Woerdman, "Orbital angular momentum of light and the transformation of Laguerre-Gaussian laser modes," Phys. Rev. A **45**(11), 8185–8189 (1992).
2. J. Courtial, K. Dholakia, L. Allen, and M. J. Padgett, "Gaussian beams with very high orbital angular momentum," Opt. Commun. **144**(4-6), 210–213 (1997).
3. G. Gibson, J. Courtial, M. Padgett, M. Vasnetsov, V. Pas'ko, S. Barnett, and S. Franke-Arnold, "Free-space information transfer using light beams carrying orbital angular momentum," Opt. Express **12**(22), 5448–5456 (2004).
4. J. Wang, J.-Y. Yang, I. M. Fazal, N. Ahmed, Y. Yan, H. Huang, Y. Ren, Y. Yue, S. Dolinar, M. Tur, and A. E. Willner, "Terabit free-space data transmission employing orbital angular momentum multiplexing," Nat. Photonics **6**(7), 488–496 (2012).
5. N. Bozinovic, Y. Yue, Y. Ren, M. Tur, P. Kristensen, H. Huang, A. E. Willner, and S. Ramachandran, "Terabit-Scale Orbital Angular Momentum Mode Division Multiplexing in Fibers," Science **340**(6140), 1545–1548 (2013).
6. Y. Yan, G. Xie, M. P. J. Lavery, H. Huang, N. Ahmed, C. Bao, Y. Ren, Y. Cao, L. Li, Z. Zhao, A. F. Molisch, M. Tur, M. J. Padgett, and A. E. Willner, "High-capacity millimetre-wave communications with orbital angular momentum multiplexing," Nat. Commun. **5**(1), 4876 (2014).
7. K. Morgan, Y. Li, W. Li, J. K. Miller, R. J. Watkins, and E. G. Johnson, "Multilevel quadrature amplitude multiplexing using coherently coupled orbital angular momentum modes," Opt. Express **26**(9), 12180–12190 (2018).
8. H. Bechmann-Pasquinucci and W. Tittel, "Quantum cryptography using larger alphabets," Phys. Rev. A **61**(6), 062308 (2000).
9. J. T. Barreiro, T.-C. Wei, and P. G. Kwiat, "Beating the channel capacity limit for linear photonic superdense coding," Nat. Phys. **4**(4), 282–286 (2008).
10. G. Vallone, V. D'Ambrosio, A. Sponselli, S. Slussarenko, L. Marrucci, F. Sciarrino, and P. Villoresi, "Free-Space Quantum Key Distribution by Rotation-Invariant Twisted Photons," Phys. Rev. Lett. **113**(6), 060503 (2014).
11. A. Mair, A. Vaziri, G. Weihs, and A. Zeilinger, "Entanglement of the orbital angular momentum states of photons," Nature **412**(6844), 313–316 (2001).
12. J. Leach, M. J. Padgett, S. M. Barnett, S. Franke-Arnold, and J. Courtial, "Measuring the Orbital Angular Momentum of a Single Photon," Phys. Rev. Lett. **88**(25), 257901 (2002).
13. J. Leach, B. Jack, J. Romero, A. K. Jha, A. M. Yao, S. Franke-Arnold, D. G. Ireland, R. W. Boyd, S. M. Barnett, and M. J. Padgett, "Quantum Correlations in Optical Angle-Orbital Angular Momentum Variables," Science **329**(5992), 662–665 (2010).
14. R. Fickler, R. Lapkiewicz, W. N. Plick, M. Krenn, C. Schaeff, S. Ramelow, and A. Zeilinger, "Quantum Entanglement of High Angular Momenta," Science **338**(6107), 640–643 (2012).
15. N. Cvijetic, G. Milione, E. Ip, and T. Wang, "Detecting Lateral Motion using Light's Orbital Angular Momentum," Sci. Rep. **5**(1), 15422 (2015).
16. S. W. Hell and J. Wichmann, "Breaking the diffraction resolution limit by stimulated emission: stimulated-emission-depletion fluorescence microscopy," Opt. Lett. **19**(11), 780–782 (1994).
17. S. Fürhapter, A. Jesacher, S. Bernet, and M. Ritsch-Marte, "Spiral phase contrast imaging in microscopy," Opt. Express **13**(3), 689–694 (2005).
18. V. D'Ambrosio, N. Spagnolo, L. Del Re, S. Slussarenko, Y. Li, L. C. Kwek, L. Marrucci, S. P. Walborn, L. Aolita, and F. Sciarrino, "Photonic polarization gears for ultra-sensitive angular measurements," Nat. Commun. **4**(1), 2432 (2013).
19. M. P. J. Lavery, F. C. Speirits, S. M. Barnett, and M. J. Padgett, "Detection of a Spinning Object Using Light's Orbital Angular Momentum," Science **341**(6145), 537–540 (2013).
20. E. Karimi, B. Piccirillo, E. Nagali, L. Marrucci, and E. Santamato, "Efficient generation and sorting of orbital angular momentum eigenmodes of light by thermally tuned q-plates," Appl. Phys. Lett. **94**(23), 231124 (2009).
21. S. Slussarenko, A. Murauski, T. Du, V. Chigrinov, L. Marrucci, and E. Santamato, "Tunable liquid crystal q-plates with arbitrary topological charge," Opt. Express **19**(5), 4085–4090 (2011).

Optics EXPRESS

22. L. Marrucci, E. Karimi, S. Slussarenko, B. Piccirillo, E. Santamato, E. Nagali, and F. Sciarrino, "Spin-to-orbital conversion of the angular momentum of light and its classical and quantum applications," J. Opt. **13**(6), 064001 (2011).
23. Y. F. Yu, Y. H. Fu, X. M. Zhang, A. Q. Liu, T. Bourouina, T. Mei, Z. X. Shen, and D. P. Tsai, "Pure angular momentum generator using a ring resonator," Opt. Express **18**(21), 21651–21662 (2010).
24. C. R. Doerr and L. L. Buhl, "Circular grating coupler for creating focused azimuthally and radially polarized beams," Opt. Lett. **36**(7), 1209–1211 (2011).
25. X. Cai, J. Wang, M. J. Strain, B. Johnson-Morris, J. Zhu, M. Sorel, J. L. O'Brien, M. G. Thompson, and S. Yu, "Integrated compact optical vortex beam emitters," Science **338**(6105), 363–366 (2012).
26. H. Huang, G. Milione, M. P. J. Lavery, G. Xie, Y. Ren, Y. Cao, N. Ahmed, T. An Nguyen, D. A. Nolan, M.-J. Li, M. Tur, R. R. Alfano, and A. E. Willner, "Mode division multiplexing using an orbital angular momentum mode sorter and MIMO-DSP over a graded-index few-mode optical fibre," Sci. Rep. **5**, 14931 (2015).
27. S. G. Leon-Saval, T. A. Birks, J. Bland-Hawthorn, and M. Englund, "Multimode fiber devices with single-mode performance," Opt. Lett. **30**(19), 2545–2547 (2005).
28. N. K. Fontaine, R. Ryf, J. Bland-Hawthorn, and S. G. Leon-Saval, "Geometric requirements for photonic lanterns in space division multiplexing," Opt. Express **20**(24), 27123–27132 (2012).
29. S. G. Leon-Saval, N. K. Fontaine, J. R. Salazar-Gil, B. Ercan, R. Ryf, and J. Bland-Hawthorn, "Mode-selective photonic lanterns for space-division multiplexing," Opt. Express **22**(1), 1036–1044 (2014).
30. S. Yerolatsitis, I. Gris-Sánchez, and T. A. Birks, "Adiabatically-tapered fiber mode multiplexers," Opt. Express **22**(1), 608–617 (2014).
31. B. Huang, N. K. Fontaine, R. Ryf, B. Guan, S. G. Leon-Saval, R. Shubochkin, Y. Sun, R. Lingle, Jr., and G. Li, "All-fiber mode-group-selective photonic lantern using graded-index multimode fibers," Opt. Express **23**(1), 224–234 (2015).
32. T. A. Birks, I. Gris-Sánchez, S. Yerolatsitis, S. G. Leon-Saval, and R. R. Thomson, "The photonic lantern," Adv. Opt. Photonics **7**, 107–167 (2015).
33. Z. S. Eznaveh, J. E. Antonio-Lopez, J. C. A. Zacarias, A. Schülzgen, C. M. Okonkwo, and R. A. Correa, "All-fiber few-mode multicore photonic lantern mode multiplexer," Opt. Express **25**(14), 16701–16707 (2017).
34. S. G. Leon-Saval, N. K. Fontaine, and R. Amezcua-Correa, "Photonic lantern as mode multiplexer for multimode optical communications," Opt. Fiber Technol. **35**, 46–55 (2017).
35. A. M. Velázquez-Benítez, J. E. Antonio-López, J. C. Alvarado-Zacarías, N. K. Fontaine, R. Ryf, H. Chen, J. Hernández-Cordero, P. Sillard, C. Okonkwo, S. G. Leon-Saval, and R. Amezcua-Correa, "Scaling photonic lanterns for space-division multiplexing," Sci. Rep. **8**(1), 8897 (2018).
36. S. Ramachandran, P. Kristensen, and M. F. Yan, "Generation and propagation of radially polarized beams in optical fibers," Opt. Lett. **34**(16), 2525–2527 (2009).
37. Y. Yue, Y. Yan, N. Ahmed, J. Y. Yang, L. Zhang, Y. Ren, H. Huang, K. M. Birnbaum, B. I. Erkmen, S. Dolinar, M. Tur, and A. E. Willner, "Mode Properties and Propagation Effects of Optical Orbital Angular Momentum (OAM) Modes in a Ring Fiber," IEEE Photonics J. **4**(2), 535–543 (2012).
38. S. Ramachandran and P. Kristensen, "Optical vortices in fiber," Nanophotonics **2**(5-6), 455–474 (2013).
39. S. G. Leon-Saval, A. Argyros, and J. Bland-Hawthorn, "Photonic lanterns," Nanophotonics **2**(5-6), 429–440 (2013).
40. A. M. Velazquez-Benitez, J. C. Alvarado, G. Lopez-Galmiche, J. E. Antonio-Lopez, J. Hernández-Cordero, J. Sanchez-Mondragon, P. Sillard, C. M. Okonkwo, and R. Amezcua-Correa, "Six mode selective fiber optic spatial multiplexer," Opt. Lett. **40**(8), 1663–1666 (2015).
41. K. Okamoto, "Preface to the Second Edition," in *Fundamentals of Optical Waveguides (Second Edition)* (Academic, 2006), pp. xv–xvi.
42. K. Shi, Y. Jung, Z. S. Eznaveh, J. C. A. Zacarias, J. E. A. Lopez, H. Zhou, R. Zhang, S. Chen, H. Wang, Y. Yang, R. A. Correa, D. J. Richardson, and B. C. Thomsen, "10×10 MDM Transmission over 24 km of Ring-Core Fibre using Mode Selective Photonic Lanterns and Sparse Equalization," in *2017 European Conference on Optical Communication (ECOC)* (2017), pp. 1–3.
43. S. Randel, A. Sierra, S. Mumtaz, A. Tulino, R. Ryf, P. J. Winzer, C. Schmidt, and R. J. Essiambre, "Adaptive MIMO signal processing for mode-division multiplexing," in *OFC/NFOEC* (2012), pp. 1–3.